

Pinch Spot Formation in High Atomic Number z Discharges

D. Mosher and D. Colombant

Plasma Physics Division, Naval Research Laboratory, Washington, D.C. 20375-5000

(Received 18 December 1991)

A nonlinear, quasi-two-dimensional model for pinch spot formation in radiation-dominated, high atomic number z pinches is presented that reproduces the experimental electrical and radiation characteristics. The high line-radiation rates of such discharges produce localized, high-density pinch spots in contrast to the spindle pinches predicted for hydrogenic discharges.

PACS numbers: 52.35.Mw

High atomic number z pinches created from megampere-level discharges in fine metal wires, dielectric fibers, and annular gas puffs have been of interest for the past twenty years as powerful laboratory sources of soft x radiation. Single-wire sources exhibit a nonlinearly developed MHD sausage instability characterized by a line of intensely emitting pinch spots with radial and axial dimensions of order 10^{-2} cm or less, separated by diffuse flares with dimensions of order 10^{-1} cm or larger [1-6]. Each spot emits 2-10-ns-wide radiation spikes, 3 to 10 of which are radiating at a given instant, with individual pinch spot impedances of order 0.1Ω . Averaged over the discharge history, these spots emit a major portion of the total x radiation and present ohm-level loads to the pulsed-power generator. Similar pinch spots are found in discharges created from multiple-wire arrays and annular gas puffs during the stagnated z -pinch phase following radial implosion [7], in x -pinch plasmas [8], in vacuum sparks [9], and discharges in liquid conductors [10]. It is shown that the high line-radiation rates of such discharges can explain the formation of pinch spots with the observed characteristics.

The nonlinear development of the sausage instability has been studied theoretically in two dimensions in dense, weakly radiating, hydrogenic z pinches [11-13]. In contrast to the compact spots observed in high atomic number (high z) discharges, these studies predict the formation of spindle pinches: extended cylindrical waists that occupy about half of the instability wavelength between flares of larger radius. Saturation of sausage modes in hydrogenic pinches by helical deformation has been proposed [14]. One-dimensional studies of high z , radiating pinches [15,16] predict radial scale lengths in the experimental range, but cannot explain the short axial scale length observed in experiments. Here, a nonlinear, quasi-2D model for pinch spot formation in radiation-dominated, high atomic number z pinches is presented that reproduces the observed short axial scale lengths and associated electrical and radiation characteristics described above. The higher line-radiation rates of high z discharges compared to the plasma-bremsstrahlung rates of hydrogenic discharges are found to be responsible for the differences in predicted pinch shapes between the two

plasma types.

A two-dimensional "gas-bag" model, originally developed to study hydrogenic pinches [13], is employed for the analysis by including the ionization and radiation characteristics of titanium [15]. In its simplest form, a constant and radially uniform current I flows inside the plasma-boundary radius $a(z,t)$ to form a pinch in radial pressure balance with the azimuthal self-magnetic field. The 2D MHD equations that describe the plasma dynamics are reduced to the single axial dimension by assuming that the particle density and radial fluid velocity vary with radius in a self-similar fashion so that their profile shapes are invariant for all times and axial locations. Though this approach is not fully consistent with Maxwell's equations, since it prescribes the current distribution rather than solving a magnetic-diffusion equation along with the dynamical equations, it allows one to study axial flow, resistivity, and radiation in a physical manner without resorting to the complexities of a full 2D radiation MHD treatment. With these assumptions, equations for conservation of particles, radial momentum, axial momentum, and energy can be written as [13]

$$\frac{\partial N}{\partial t} + \frac{\partial}{\partial z}(Nv_z) = 0, \quad (1)$$

$$I^2 = 2(1+Z)NkT, \quad (2)$$

$$MN \left[\frac{\partial v_z}{\partial t} + v_z \frac{\partial v_z}{\partial z} \right] = \frac{I^2}{a} \frac{\partial a}{\partial z}, \quad (3)$$

$$-\frac{I^2}{a} \frac{\partial a}{\partial t} - \left(\frac{5}{4} - \delta\right) I^2 \frac{\partial v_z}{\partial z} = P_r - P_\Omega \left[1 + \left(\frac{\partial a}{\partial z} \right)^2 \right]. \quad (4)$$

In the above equations, $N(z,t)$ is the ion line density (integral of density over the cross-sectional area), $T(z,t)$ and $v_z(z,t)$ are the radially uniform temperature and axial fluid velocity, $Z(T)$ is the ionization state, M is the ion mass, $\delta(T)$ is a correction due to variable ionization to the term containing the ratio of specific heats for an ideal gas, axial heat conduction transverse to the strong B field is ignored, and electromagnetic cgs units are employed. The quantities P_r and P_Ω are radially integrated radia-

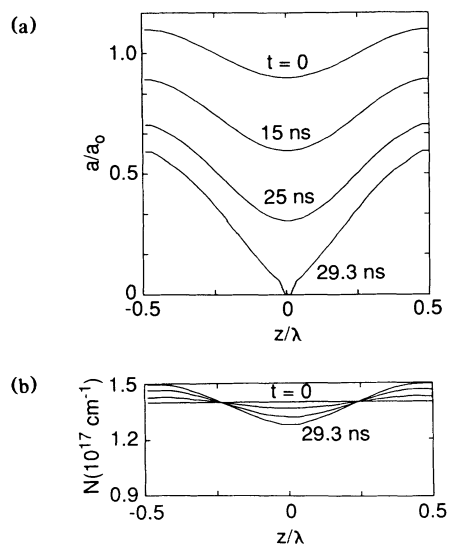


FIG. 1. (a) Envelope radius distributions from the gas-bag model at various times for the numerical example discussed in the text. (b) Line density distributions from the gas-bag model at corresponding times.

tion and Ohmic heating rates (power/length) given by [16]

$$P_r = 2\pi a \sigma T^4 (1 - e^{-a}) [1 + e^{-a} - (1 - e^{-a})/a], \quad (5)$$

$$P_n = \eta I^2 / \pi a^2. \quad (6)$$

The term in brackets on the right-hand side of Eq. (4) arises from the axial and radial current-flow contributions to Ohmic heating. The optical depth a can be approximated by $(a_i/a)^3$, where $a_i = (ZSN^2/2\pi^2\sigma T^4)^{1/3}$ is the radius at which blackbody radiation from the surface of the discharge $P_b = 2\pi a \sigma T^4$ equals optically thin radiation from the volume $P_t = ZSN^2/\pi a^2$, and $S(T)$ is the optically thin radiation rate coefficient [15]. With these definitions, P_r approaches P_t (or P_b) for small (or large) values of a . Spitzer resistivity transverse to a strong magnetic field is chosen for $\eta(T)$.

The above system of equations has been solved numerically in an initially stationary titanium plasma with uniform line density N_0 and a perturbed plasma radius $a(z,0) = a_0[1 - \epsilon \cos(2\pi z/\lambda)]$. Examples of the time evolutions of boundary radius and line density over one axial wavelength of the perturbation are shown in Fig. 1 for $N_0 = 1.4 \times 10^{17} \text{ cm}^{-1}$, $a_0 = 0.3 \text{ cm}$, $2\pi a_0/\lambda = 1$, $\epsilon = 0.1$, and $I = 1 \text{ MA}$. For these plasma conditions [15], $T \approx 1 \text{ keV}$, $Z \approx 20$, $\beta = P_t/P_n \approx 100$, and $a_i \approx 1 \times 10^{-2} \text{ cm}$. The figure shows collapse to a spot of small radial and axial extent within which there is a slight reduction in line density. As observed in experiments [1,4,5], the small reduction in N corresponds to a large increase in spot density and, through Eq. (2), a slight increase in spot temperature compared to the surrounding plasma.

The V-shaped profile displayed in Fig. 1 contrasts with

the U-shaped profiles obtained in other works [11,12], and with the same gas-bag model treating weakly radiating, hydrogenic discharges [13]. The strong density concentration at the base of the V shape gives rise to the observed [1-5] highly localized radiation spots. The U-shaped profile characteristic of hydrogenic discharges leads to radiation emission along a line of much greater axial extent. The shape difference can be explained by magnitude ordering of the conservation equations. Equation (3) has flow-velocity solutions in two regimes determined by the ratio of sound speed $c_s = [(1+Z)kT/M]^{1/2}$ to λ/τ , where τ is a characteristic time for radial variations, and Eq. (2) has been used to eliminate I^2 . When $\lambda/\tau > c_s$, $v_z \approx c_s^2 \tau / \lambda < \lambda/\tau$ and the variation of N in time and space is estimated to be small from Eq. (1). This case applies to the present calculations where heating by rapid radial compression is required to balance large line-radiation losses. The V-shaped profile results from the inability of significant mass to void the tightly pinched region during rapid compression. For weakly radiating hydrogenic pinches with comparable dimensions and discharge parameters, slower radial motion combined with more rapid axial flow suffices for energy balance, $v_z \approx c_s > \lambda/\tau$, large reduction of N is predicted in the compressed region, and the U-shaped profile results.

The small computed axial variation of N in the present work allows one to approximate the evolution of $a(z,t)$ by neglecting axial gradients. One is left with Eq. (2) and

$$\frac{I^2}{a} \frac{\partial a}{\partial t} = P_n - P_r. \quad (7)$$

Since $P_r \approx P_t \gg P_n$ for $a > a_i$, neglecting P_n and integrating Eq. (7) leads to

$$a^2/a_0^2 = [1 - \epsilon \cos(2\pi z/\lambda)]^2 - t/\tau_r, \quad (8)$$

where the characteristic radiation collapse time $\tau_r = \pi I^2 a_0^2 / 2ZSN^2$ is 36.2 ns for the above numerical example. As $a(z,t)$ approaches a_i , Eq. (7) predicts that collapse continues into the optically thick regime until $P_b = P_n$ at an equilibrium radius $a_f = a_i/\beta^{1/3} = (\eta I^2 / 2\pi^2 \sigma T^4)^{1/3}$. For the above numerical example, a_f is about 20 μm .

Figure 2 demonstrates the good fit of Eq. (8) to the numerical solution shown in Fig. 1 for the same initial perturbation and displayed t/τ_r values. Equations (5) and (8), plus the limit $a(z,t) \geq a_f$, can then be used to calculate the axial distribution of radiation intensity as a function of time. Figure 3 shows P_r , normalized to the radiation rate of a blackbody with radius a_f , for $\beta = 64$ and at the times $t = [(1-\epsilon)^2 - a^2(0,t)/a_0^2] \tau_r$ when $a(0,t) = 2a_i$, a_i , and a_f . The double-peak distribution for the fully collapsed center arises because the plasma continues to emit like a blackbody as the radius increases from a_f to a_i on either side of $z=0$. During the time interval of maximum radiation intensity, i.e., when $a_f \leq a \leq a_i$,

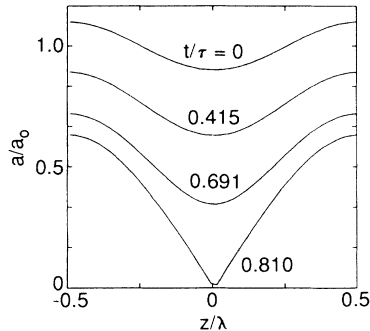


FIG. 2. Envelope radius distributions from Eq. (8) for t/τ_r values corresponding to Fig. 1(a).

one-half of the total radiation emitted within a wavelength of the discharge comes from a central collapsed region of axial extent $\Delta z/\lambda \approx 1.5a_f/a_0$, where Δz is insensitive to the value of β . The diameter at the edges of this region is about $3a_f$, so that axial and radial dimensions of the intensely radiating region are of order $100 \mu\text{m}$ for a range of experimental discharge parameters.

As time progresses beyond $(1 - \epsilon)^2\tau_r$, Eq. (8) predicts that the central fully collapsed region spreads axially until $t \approx (1 + \epsilon)^2\tau_r$ when the entire length of the discharge is at radius a_f . However, the assumption of constant discharge current must break down during the spreading collapse since a fully collapsed plasma would have an electrical load impedance and radiated power orders of magnitude higher than those of the pulsed power generator. At most, the load impedance and dissipated power can approach the 0.1-1- Ω , 1-10-TW driving-generator values before collapse is disrupted. The dynamic impedance of the collapsing discharge can be estimated by noting that Eq. (7) provides local power balance between radiation losses, compressional work on the plasma (electrical energy coupled to a time-varying inductance), and resistive heating. The integral of P_r over a wavelength of the perturbation is therefore equal to the instantaneous impedance $Y(t)$ of discharge length λ , or

$$Y(t) = \frac{1}{I^2} \int_{-\lambda/2}^{\lambda/2} P_r dz = \frac{2\pi a_f \lambda \sigma T^4}{I^2} R(t) = \frac{Z^{1/3} T(\text{eV})^{13/6} \lambda}{7.4 \times 10^4 I(\text{MA})^{4/3}} R(t). \quad (9)$$

Here, $R(t)$ is the power radiated in a wavelength normalized to that of a fully collapsed discharge, and practical units have been employed on the right-hand side to express $Y(t)$ in ohms. The time variation of $R(t)$ is shown in Fig. 4 for $\epsilon = 0.1$, $a_f/a_0 = 4 \times 10^{-3}$, and three values of β . For $t/\tau_r \leq (1 - \epsilon)^2$, $R(t)$ is controlled by radial collapse to a spot. For greater times, the impedance variation is controlled by axial spreading of the collapsed region. Examination of Eq. (8) and the integral demonstrate that $R(t)$ variations during radial collapse for other parameter values are close to the displayed curves for

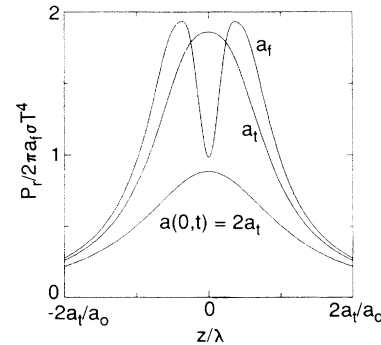


FIG. 3. Radiation distributions normalized to that of a blackbody with radius a_f , for $\beta = 64$, $\epsilon = 0.1$, and at the times when $a(0,t) = 2a_t$, a_t , and a_f .

similar values of $\beta(a_f/a_0)^2$. The coefficient of $R(t)$ in Eq. (9) is about 1Ω for $\lambda = 0.3 \text{ cm}$, I in the range of 1-10 MA, and associated T values of 300-1000 eV.

Experiments with 3-cm-long, single high z wire discharges showed that 10 to 30 spots are created during a 40-ns-long x-radiation pulse [1,5]. The pulse is typically composed of 2-10-ns radiation spikes from individual pinch spots, 3 to 10 of which are radiating at a given instant. The time-averaged impedance of the discharge was measured [6] to remain constant at 1Ω as the driving voltage and discharge current were varied over a factor of 2.5. Therefore, individual pinch spot impedances achieved values of order 0.1Ω , i.e., $R(t) \approx 0.1$, before disruption. Comparing these data to Fig. 4, $R(t)$ exceeds 0.1 before significant axial spreading of the pinch occurs, so that pinch spots with axial dimensions much in excess of Δz could not occur without exceeding the generator capabilities. The analysis is therefore consistent with the experimental observation of intensely radiating spots with axial and radial dimensions of order $100 \mu\text{m}$. The short measured durations of individual x-ray spikes are consistent with the rapid rise of radiation intensity indicated in the figure. Since electric fields $IY/\Delta z \approx 10\text{-}100 \text{ MV/cm}$ can be associated with each pinch spot, the

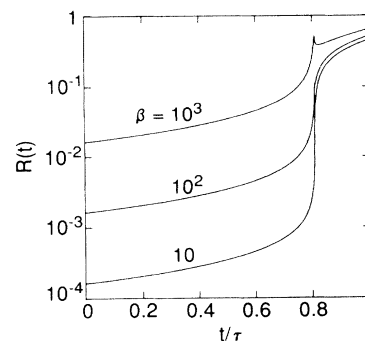


FIG. 4. The time variation of normalized discharge impedance for $\epsilon = 0.1$, $a_f/a_0 = 4 \times 10^{-3}$, and three values of β .

mechanism presented here can explain observations of nonthermal x rays [1,3,4] due to high-energy electrons. In addition, the observed ability of the discharge to match impedance with the generator under varying conditions conforms to the notion that the radiation-driven dynamics allows the pinch spots to collapse until resistive loading limits the discharge current.

This work was supported by the Office of Naval Research.

[1] D. Mosher *et al.*, *Appl. Phys. Lett.* **23**, 429 (1973).

[2] C. Stallings, K. Nielson, and R. Schneider, *Appl. Phys. Lett.* **29**, 404 (1976).

[3] C. M. Dozier *et al.*, *J. Phys. B* **10**, L73 (1977).

[4] T. Nash *et al.*, *J. Quant. Spectrosc. Radiat. Transfer* **44**, 485 (1990).

[5] N. Loter *et al.*, *J. Quant. Spectrosc. Radiat. Transfer* **44**,

509 (1990).

[6] D. Mosher *et al.*, *Ann. N.Y. Acad. Sci.* **251**, 632 (1975).

[7] N. R. Pereira and J. Davis, *J. Appl. Phys.* **64**, R1 (1988).

[8] D. A. Hammer *et al.*, *Appl. Phys. Lett.* **57**, 2083 (1990).

[9] B. S. Fraenkel and J. L. Schwob, *Phys. Lett.* **40A**, 83 (1978).

[10] W. Lochte-Holtgreven, *Atomkernenergie* **28**, 150 (1976).

[11] D. L. Book, E. Ott, and M. Lampe, *Phys. Fluids* **19**, 1982 (1976).

[12] V. V. Vikhrev, V. V. Ivanov, and G. A. Rozanova, *Fiz. Plazmy* **15**, 77 (1989) [*Sov. J. Plasma Phys.* **15**, 44 (1989)].

[13] D. Colombant and D. Mosher, in *Dense Z-Pinches*, edited by N. R. Pereira, J. Davis, and N. Rostoker, AIP Conf. Proc. No. 195 (AIP, New York, 1989), p. 191.

[14] N. A. Salingaros, *Phys. Scr.* **43**, 416 (1991).

[15] D. Mosher and D. Colombant, in *Dense Z-Pinches* (Ref. [13]), p. 262.

[16] V. N. Dokuka and A. A. Samokhin, *Fiz. Plazmy* **15**, 460 (1989) [*Sov. J. Plasma Phys.* **15**, 267 (1989)].